Submitted to *Analytical Chemistry* 3/31/11

Brominated Tyrosine and Polyelectrolyte Multilayer Analysis by Laser Desorption VUV Postionization and Secondary Ion Mass Spectrometry

Melvin Blaze M.T.,[1] Lynelle K. Takahashi,[2,3] Jia Zhou,[3,∫] Musahid Ahmed,[3] Gerald L. Gasper,[1] F. Douglas Pleticha,[1] and Luke Hanley[1,*]

[1]Department of Chemistry, University of Illinois at Chicago, Chicago, IL 60607

[2]Department of Chemistry, University of California, Berkeley, Berkeley, CA 94720

[3]Chemical Sciences Division, Lawrence Berkeley National Laboratory, Berkeley, CA 94720

Abstract

The small molecular analyte 3,5-dibromotyrosine (Br_2Y) and chitosan-alginate polyelectrolyte multilayers (PEM) with and without adsorbed Br_2Y were analyzed by laser desorption postionization mass spectrometry (LDPI-MS). LDPI-MS using 7.87 eV laser and tunable 8 – 12.5 eV synchrotron vacuum ultraviolet (VUV) radiation found that desorption of clusters from Br_2Y films allowed detection by ≤8 eV single photon ionization. Thermal desorption and electronic structure calculations determined the ionization energy of Br_2Y to be ~8.3±0.1 eV and further indicated that the lower ionization energies of clusters permitted their detection at ≤8 eV photon energies. However, single photon ionization could only detect Br_2Y adsorbed within PEMs when using either higher photon energies or matrix addition to the sample. All samples were also analyzed by 25 keV Bi_3^+ secondary ion mass spectrometry (SIMS), with the negative ion spectra showing strong parent ion signal which complemented that observed by LDPI-MS. The negative ion SIMS depended strongly on the high electron affinity of this specific analyte and the analyte's condensed phase environment.

*Corresponding author, email: LHanley@uic.edu

∫Current address: Chemistry Department, Brookhaven National Laboratory, Upton, NY

I. INTRODUCTION

Bacterial biofilms consist of colonies of microbial cells embedded in an extracellular polysaccharide matrix which are often attached to solid surfaces.[1] They are responsible for a large number of medical infections and play a role in environmental and industrial processes. The structure and composition of these microbial biofilm communities depend on the properties of their anchoring surface since the metabolism of individual microbes is affected by their environment. Given that even a single species biofilm is composed of microbial cells in different metabolic states, imaging of intact biofilms will provide chemical information not available to studies of homogenized microbial extracts.

Mass spectrometric (MS) imaging can probe chemical distributions of metabolites and signaling molecules within intact bacterial biofilms to help elucidate the role of metabolic state and environment. Secondary ion mass spectrometry (SIMS) is one MS imaging method that has been applied to bacterial biofilms and other intact biological tissue.[2-5]

The authors are developing two other methods for MS imaging analyses of bacterial biofilms and other samples: laser desorption postionization mass spectrometry (LDPI-MS)[6,7] and secondary neutral mass spectrometry (SNMS).[8,9] Both methods rely upon vacuum ultraviolet (VUV) single photon ionization (SPI) of laser desorbed or ion sputtered neutrals.[10] Recent LDPI-MS work has focused on SPI with 7.87 eV VUV radiation because it is available from a convenient laboratory source – the molecular fluorine laser which emits at 157.6 nm. However, its 7.87 eV photon energy is below the ionization energy of many analytes, limiting the potential targets that it can ionize. 10.5 eV VUV radiation from the 118 nm ninth harmonic of the Nd:YAG laser has historically been the most popular VUV source for SPI because of its ability to ionize a much larger class of molecular analytes while avoiding detection of water, carbon

dioxide and other abundant species usually of little interest to MS imaging.[10] However, the 10.5 eV source suffers from a relatively low, ~nJ energy per pulse which limits sensitivity and precludes its use in commercial instruments.

The question arises as to what VUV photon energies are most effective for postionization. Photon energies that are slightly above the ionization threshold of a molecular analyte have most often been considered ideal for LDPI-MS as they minimize the excess energy available for parent ion dissociation.[9,10] Different photon energies for SPI can readily be accessed at a VUV synchrotron light source.[7,8,11,12]

Another issue that arises in MS imaging is the difficulty of establishing analysis protocols on complex, heterogeneous biological samples. This difficulty has led to the use of organic multilayer models to evaluate the suitability of SIMS protocols for analysis of intact biological samples. SIMS studies of organic multilayer models have included Langmuir-Blodgett films of barium arachidate,[13] dipalmitoyl-phosphatidylcholine-sucrose multilayers[14] and peptide doped trehalose thin films.[3]

A polyelectrolyte multilayer (PEM) model was applied here that is particularly well-suited to evaluate MS imaging protocols for bacterial biofilms. This PEM was composed of alginate and chitosan, two high molecular weight biopolymers which simulate the extracellular polysaccharides of biofilms. These PEMs were prepared by electrostatic layer by layer assembly of these two oppositely charged polysaccharides.[15] This model also allowed introduction of small molecular analytes into the PEM, simulating the presence of metabolites, signaling molecules, and other species present within actual biofilms. Here, the small molecular analyte was 3,5-dibromotyrosine (Br_2Y), which was electrostatically adsorbed to every alternating alginate layer

of the PEM. The presence of bromine and the unique isotopic pattern of Br_2Y facilitated identification by MS.

This study examined LDPI-MS of neat Br_2Y films, neat PEMs, and PEMs with adsorbed Br_2Y (Br_2Y-PEMs). 25 keV Bi_3^+ SIMS was also performed on these samples, given the several prior studies that used SIMS to study biofilms.[2-5] MS analysis was performed using a commercial SIMS instrument additionally configured for LDPI-MS by coupling to a desorption laser and a tunable VUV synchrotron beamline.[7,8,16] Samples were also analyzed with a home built LDPI-MS that utilized a 7.87 eV molecular fluorine laser for postionization.[6] Ionization energies (IEs) of Br_2Y were determined experimentally and compared to IEs from electronic structure calculations. The results are discussed in terms of SPI mechanisms and desorption of Br_2Y, both from neat films and PEMs.

II. EXPERIMENTAL DETAILS

A. Preparation and Verification of Br_2Y films, PEMs, and Br_2Y-PEMs. Br_2Y films were prepared from solutions in (1:1 v:v) acetonitrile:water that were dried on gold-coated silicon substrates.

PEMs were prepared on gold-coated substrates as described previously.[15,17] PEMs were verified by attenuated total reflection Fourier transform infrared spectroscopy. Elemental content of the PEMs was determined by monochromatic X-ray photoelectron spectroscopy using instrumentation and procedures previously described.[18] Details of the preparation and verification of the PEMs are given in Supporting Information.

20 mg/ml α-cyano-4-hydroxycinnamic acid (CHCA) matrix solutions were prepared in (7:3 v:v) acetonitrile:trifluoroacetic acid (0.1% v:v). These matrix solution were then sprayed onto a subset of the PEMs to facilitate desorption during 7.87 eV LDPI-MS.

B. 8 – 12.5 eV Synchrotron LDPI-MS and SIMS. Synchrotron LDPI-MS and SIMS were recorded using a commercial SIMS instrument (TOF.SIMS 5, ION-TOF Inc., Munster, Germany) using 25 keV Bi_3^+ primary ions.[8] The SIMS instrument was modified for LDPI-MS by the addition of a 349 nm pulsed desorption laser (Explorer, Newport) operating at 2500 Hz with a spot size of ~30 μm diameter and typical laser desorption peak power density of 1 to 10 MW/cm^2. The laser desorbed neutral molecules were photoionized by 8.0 to 12.5 eV tunable VUV synchrotron radiation from the Chemical Dynamics Beamline at the Advanced Light Source (Lawrence Berkeley National Laboratory, Berkeley, CA)[16] 143,000 laser shots on a single spot were used for each displayed mass spectrum. This instrument was also used to record photoionization efficiency curves of gas phase Br_2Y molecules. See Supporting Information for further details.

C. 7.87 eV Laser LDPI-MS. 7.87 eV laser LDPI-MS was collected using a custom built instrument at the University of Illinois at Chicago which is equipped with a 157.6 nm pulsed laser (7.87 eV) for photoionization and was described in detail previously.[6] This LDPI-MS has a 349 nm Nd:YLF desorption laser operating at 100 Hz, with a spot size of ~20 μm diameter and typical desorption laser peak power density ranging from 30 to 70 MW/cm^2. The sample was rastered at 100 μm/s with respect to the laser, so each 20 μm sample spot was sampled by ~20 desorption laser shots and a total of 50 – 100 laser shots were sufficient to obtain spectra with optimal signal to noise. See Supporting Information for further details.

D. Electronic Structure Calculations. Calculations were performed using density functional theory with a commercial quantum chemistry software package (Gaussian 03, Pittsburgh, PA).[19] Vertical ionization energies (IEs) were calculated for Br_2Y, $[Br_2Y]_2$, $[Br_2Y][H_2O]$ and $[Br_2Y][H_2O]_3$ (see Supporting Information for geometries and other details).

The $[Br_2Y][H_2O]_3$ cluster was chosen as an intermediate species representative between what is expected to be highly abundant $[Br_2Y][H_2O]$ and the much larger clusters thought to form in MALDI.[20,21]

III. RESULTS AND DISCUSSION

A. Single Photon Ionization of Evaporated and Laser Desorbed Br_2Y Films. The first experiments were designed to evaluate VUV SPI of Br_2Y. The photoionization efficiency curve of evaporated Br_2Y (see Supporting Information) was recorded by monitoring the parent ion at m/z 337 while sweeping the VUV photon energy from the synchrotron. The experimental IE of Br_2Y of 8.3±0.1 eV was determined from the extrapolation of the photoionization efficiency curve using the drawn lines and agreed well with the 8.3 eV IE determined by electronic structure calculations.

Next, Br_2Y films on gold-coated substrates were laser desorbed and the resultant gaseous neutrals photoionized by VUV radiation and detected by time-of-flight MS. Figure 1 displays the LDPI-MS of Br_2Y films recorded using both 7.87 eV laser and 8.0 eV synchrotron photoionization. Both display characteristic fragments and clusters of Br_2Y. All Br-containing peaks are referred to below by their lowest mass isotopes (i.e., those composed of ^{12}C, ^{79}Br, and ^{1}H) and were verified by the unique 1:0.97 isotopic pattern for ^{79}Br:^{81}Br (see below).

Control experiments showed no significant ion signal from Br_2Y films except in the presence of both VUV radiation and the desorption laser (LD). This fact was demonstrated by the data in Figure 1 labeled “VUV only” and “LD only”, neither of which display any significant ion signal. Thus, few volatile species were detected by SPI at room temperature in the absence of laser desorption and little direct ionization occurred in the sole presence of the desorption laser.

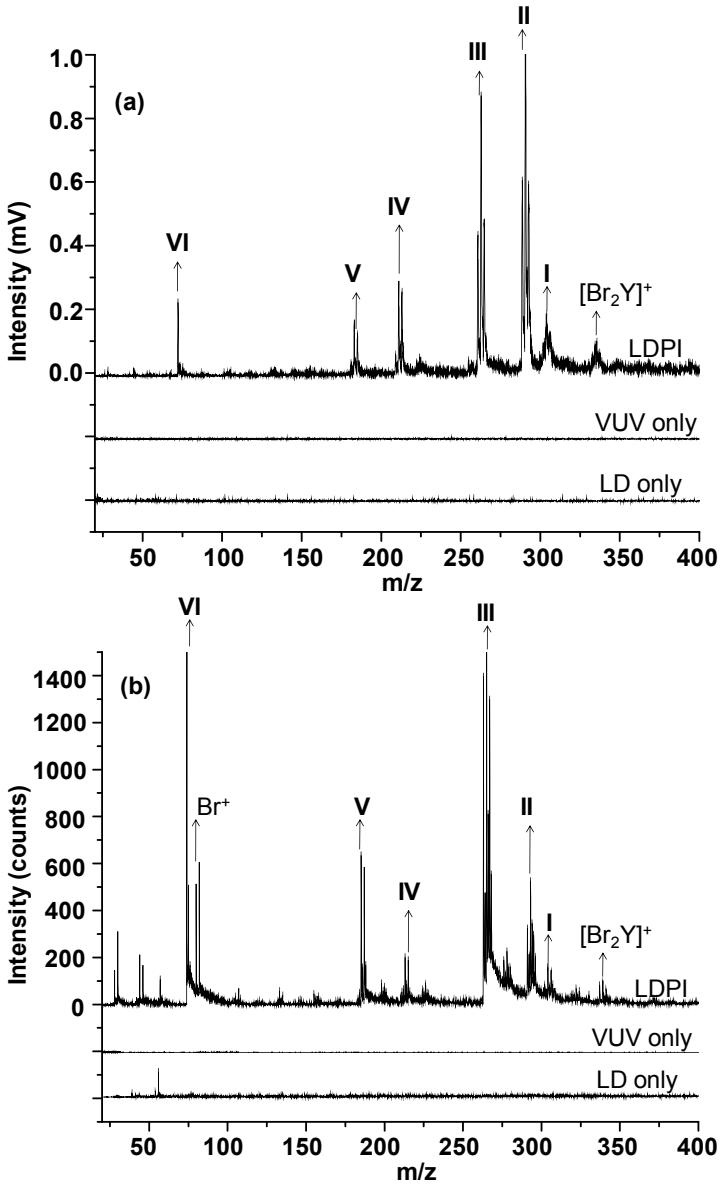

Figure 1. (a) 7.87 eV laser and (b) 8.0 eV synchrotron LDPI-MS of Br_2Y films: low mass range. The fragment ion structures associated with the Roman numeral labels are given in Figure 2.

The $[Br_2Y]^+$ parent ion at m/z 336.9 along with various low mass fragments of Br_2Y appear in both the both 7.87 eV laser and 8.0 eV synchrotron LDPI-MS in Figure 1. Figure 2 identifies each of these fragments by a Roman numeral and illustrates the proposed fragment structures. M/z 302.9 (I) was attributed to the parent ion after loss of H_2O_2. M/z 291.9 (II) was attributed to loss of COOH via cleavage of the α C-C bond. M/z 264.0 (III) was attributed to loss of $NH_2CHCOOH$ via cleavage of the β C-C bond. These observations were consistent with prior

VUV SPI studies that found amino acids predominantly undergo cleavage via the C-C bonds that are α and β to the terminal carboxyl group.[22-25] M/z 213.0 (IV) and m/z 185.1 (V) underwent similar cleavages with the additional loss of Br (losses of BrCOOH and $BrNH_2CHCOOH$, respectively). The charge resided on the aromatic group for most of these fragment ions due to charge stabilization via delocalization.[24] Proton transfer occurred for only two of the fragment ions observed, III and V. However, some fraction of β C-C bond cleavage led to the charge residing on the carboxyl group and produced the m/z 74.0 (VI) ion.

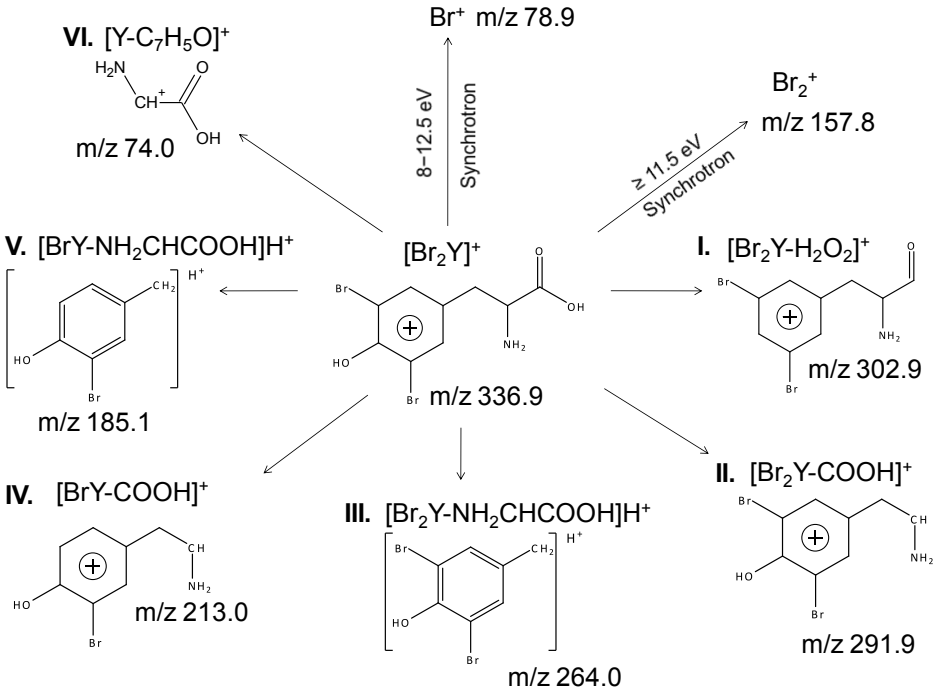

Figure 2. Schematic diagram of the fragmentation of Br_2Y by 7.87 eV laser and 8 - 12.5 eV synchrotron LDPI-MS, with Roman numerals identifying fragment ions. Br^+ and Br_2^+ were only observed by synchrotron photoionization at the noted photon energies.

Some differences were observed between LDPI-MS using 7.87 eV laser and 8.0 eV synchrotron photoionization. The relative abundances of fragment ions differed with photoionization source and desorption conditions. M/z 291.9 (II) appeared as the most intense peak by 7.87 eV laser photoionization while m/z 264.0 (III) was the most intense peak by 8.0 eV

synchrotron photoionization. However, the most significant difference was the sole appearance of Br^+ in the 8.0 eV synchrotron photoionization, as discussed further below.

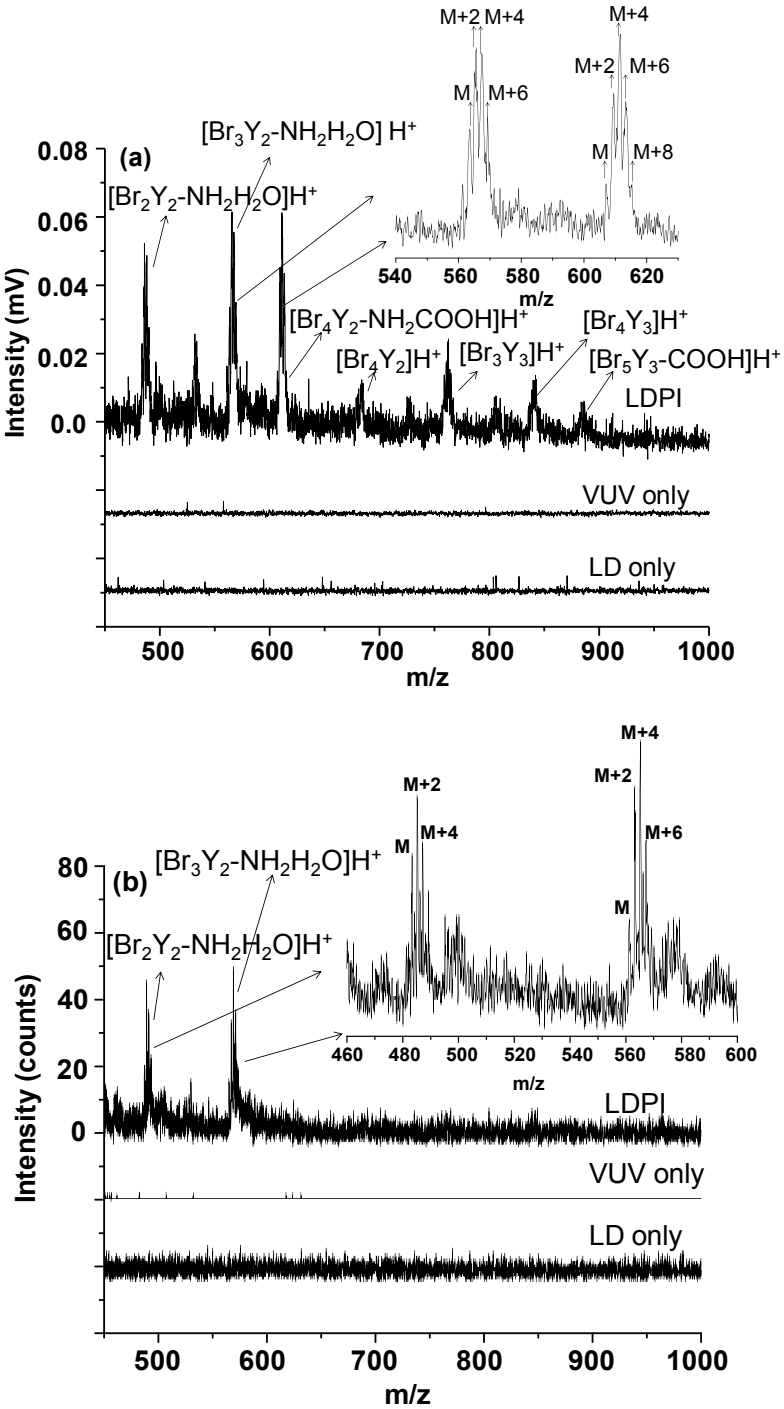

Figure 3. (a) 7.87 eV laser and (b) 8.0 eV synchrotron LDPI-MS of Br_2Y films: high mass range.

Certain higher mass ions attributed to clusters of Br_2Y were also observed at both 7.87 eV laser and 8.0 eV synchrotron photoionization energies, as shown in Figure 3. The peak envelope in Figure 3(a) at m/z 561.8, 563.8, 565.8, and 567.8 with peak intensity ratios 1:3:3:1 matched with m/z and isotopic distribution for $[Br_3Y_2\text{-}NH_2H_2O]H^+$, the dimer of Br_2Y after loss of Br, NH_2, and H_2O. The other cluster at m/z 482.9 was assigned as $[Br_2Y_2\text{-}NH_2H_2O]H^+$. These clusters were detected by both 7.87 eV laser and 8.0 eV synchrotron photoionization.

The appearance of the aforementioned ions in Figure 3 confirmed cluster formation during laser desorption from pure films of Br_2Y. Pure analyte and analyte/solvent cluster formation also explained the appearance of ion signal for the parent ion and fragments thereof (Figures 1a and 2), despite the fact that the 7.87 photon energy was lower than the ~8.3 eV experimental IEs of Br_2Y. Electronic structure calculations found IEs of 7.8 eV for $[Br_2Y]_2$, 8.1 eV for $[Br_2Y][H_2O]$ and 7.9 eV for $[Br_2Y][H_2O]_3$. These calculated IEs indicate that clustering between Br_2Y monomers or with water lowered their IEs below that of the monomer. Thus, the lower IEs of pure Br_2Y clusters and/or $[Br_2Y]_m[H_2O]_{n>1}$ and their dissociation following photoionization enabled the detection of Br_2Y by 7.87 eV laser LDPI-MS, leading to essentially all of the ion signal observed in both Figures 1a and 3a.

Molecular dynamics simulations and experimental probes of the evolution of a desorption plume in the MALDI process showed that pulsed laser irradiation results in the ejection of a mixture of individual molecules, clusters, and microdroplets.[20,21] Previous studies also showed that IEs of clusters of pure analyte or analyte-solvent are substantially lower than their corresponding monomers. For example, clusters of proline and 2,5-dihydroxybenzoic acid displayed lower IEs than the free matrix or proline[26] as did cytosine dimers compared to

monomers[27] and water clusters compared to isolated water molecules.[28,29] All of this prior work supports the cluster desorption/photoionization mechanism proposed here.

Another aspect of the clusters that Br_2Y forms with itself and/or water was that many, if not all, were protonated. Prior SPI of formic acid and water clusters found that protonated species dominated.[28,30] The two cluster species detected by both laser and synchrotron VUV SPI, $[Br_2Y_2\text{-}NH_2H_2O]H^+$ and $[Br_3Y_2\text{-}NH_2H_2O]H^+$, were both protonated. Thus, all higher mass clusters observed solely in laser VUV SPI were also assigned as protonated, although their signal to noise ratios were insufficient to assign m/z values with <1 m/z accuracy.

The 7.87 laser LDPI-MS show a ~0.05 ratio of clusters to fragments (as defined in Figure 2), indicating the dominance of the fragments in the spectra. The low excess energy available from threshold single photon ionization at 7.87 eV of clusters seems insufficient to break covalent bonds within Br_2Y. This is supported by the 9.45 eV SPI-MS of evaporated Br_2Y, which showed little fragmentation (see Supporting Information). The excessive fragmentation as well as differences in fragmentation pathways between ≤8.0 eV LDPI-MS and SPI-MS indicated that protonation after cluster photoionization led to lower energy dissociation pathways that allowed formation of at least some of the fragment ions depicted in Figure 2. However, further experiments and calculations are required to further elucidate the fragmentation mechanism.

The low photon energy and narrow bandwidth of the 7.87 eV laser support the ionization mechanism via lowered cluster IEs. However, the case with the 8.0 eV synchrotron LDPI-MS of the Br_2Y films in Figures 1b and 3b is less clear. The slightly higher 8.0 eV photon energy and the 0.2 eV bandwidth of the synchrotron radiation[16] left open the possibility of some threshold single photon ionization of Br_2Y and $[Br_2Y][H_2O]$. Furthermore, some signal may have resulted from a minor amount of photoelectron ionization[31] or higher VUV harmonics leaking through

the gas filter in the synchrotron beamline causing photoionization, as discussed previously.[32] However, the similarity of the fragments and clusters for both 7.87 eV laser and 8.0 eV synchrotron radiation and the similar cluster to fragment ratios (except as noted below) argued for a common ionization mechanism.

Nevertheless, there were several significant differences between 7.87 eV laser and 8.0 eV synchrotron radiation of Br_2Y films. The high mass Br_2Y spectra showed a higher mass distribution of clusters for 7.87 eV laser photoionization. These higher mass clusters included the intact protonated dimer, $[Br_4Y_2]H^+$, the trimer after a single Br loss, $[Br_5Y_3]H^+$, and fragments thereof. The source of this difference was not determined, but likely resulted from differences in either desorption/ionization conditions and/or TOF collection/transmission efficiencies between the two instruments.

Another significant difference between the Br_2Y spectra from the two photoionization sources was the observation of a peak at m/z 78.9 due to Br^+ only for 8.0 eV synchrotron photoionization (Figure 1). This result led to experiments in which the tunability of synchrotron radiation was exploited to record the LDPI-MS of Br_2Y films at photon energies above 8.0 eV (see Supporting Information). Increasing the photon energy from 8.0 to 12.5 eV showed only modest changes in the fragmentation pattern for Br_2Y, which remained different from those of 11.5 eV SPI-MS of evaporated Br_2Y. However, the signal intensity for all fragments did increase with photon energy, presumably due to a corresponding increase in the photoionization cross sections of the desorbed clusters.

Intense signals for both Br^+ at m/z 78.9 and Br_2^+ at m/z 157.8 were observed at photon energies in excess of their ionization energies of 11.81 and 10.52 eV, respectively. The 349 nm wavelength of the desorption laser is sufficient to induce photodissociation of various organic

bromides via the C−Br bond whose ~3 eV bond energy is readily cleaved to form bromine and hydrogen radicals.[33,34] Br_2 could have formed from surface adsorbed Br that recombined during laser induced thermal desorption, analogous to the formation of O_2 by laser induced thermal desorption of atomic oxygen on metal surfaces.[35] Examination of the time evolution of the Br and Br_2 signal (data of spectra versus laser shot recorded from a single sample spot not shown) indicated a relative increase in their signal over time compared to the Br_2Y fragment ions and clusters. This time evolution supported a Br_2Y degradation mechanism for the formation of Br and Br_2. This degradation might also explain some of the differences in fragment ratios between laser and synchrotron photoionization.

Neither Br nor Br_2 was detected by 7.87 laser photoionization (see Figure 1). Br_2^+ was only observed by synchrotron photoionization with photon energies at and above the 10.52 eV Br_2 IE. However, Br^+ was observed with 8.0 eV synchrotron radiation and at other photon energies below the 11.81 eV ionization energy of the Br atom: it may have formed by the same low photon energy mechanisms discussed above for the experiments using synchrotron radiation.

B. LDPI-MS of Polyelectrolyte Multilayers: Neat PEMs and Br_2Y-PEMs. The above results established the ability of VUV SPI to detect Br_2Y as neat films, so the next step was to examine the conditions required to detect Br_2Y adsorbed into PEMs. These Br_2Y-PEMs and also neat PEMs (without Br_2Y) were analyzed by LDPI-MS using both 7.87 eV laser and 11.5 eV synchrotron photoionization, with the higher photon energy chosen at the synchrotron for its large expected photoionization cross sections.

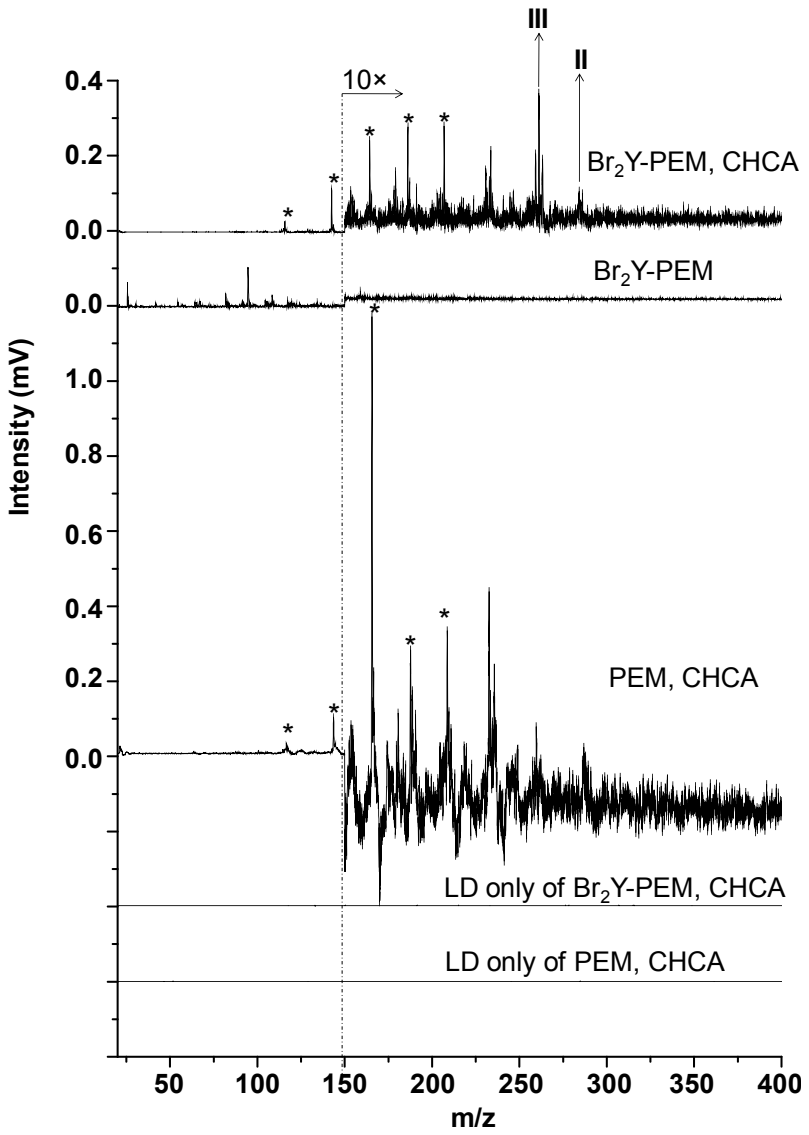

Figure 4. 7.87 eV laser LDPI-MS of Br_2Y-PEM (top trace) with CHCA matrix; (second trace from top) without CHCA, but with Br_2Y; and (third trace from top) with CHCA, but without Br_2Y. The corresponding LD only of samples containing matrix are also shown. CHCA-only associated peaks marked with asterisks.

Figure 4 shows 7.87 eV laser LDPI-MS of Br_2Y-PEMs, analyzed with and without CHCA matrix added to the fully prepared multilayer prior to MS analysis. The CHCA-treated sample allowed matrix-assisted laser desorption of neutral species, which produced m/z 264.0 (III) and m/z 291.9 (II) ions upon single photon ionization. These two ions were previously observed as the most intense ions formed from the neat Br_2Y films (see Figures 1 and 2). The ion

observed at m/z 189.0 in Figure 4 was attributed to the CHCA parent ion and m/z 210 was attributed to the $[CHCA{\cdot}Na]^+$ complex while m/z 145.6 and several lower m/z peaks were assigned as CHCA fragments. All CHCA-only peaks are marked with asterisks in Figure 4.

The spectrum of the Br_2Y-PEM without matrix shows no Br_2Y-attributed peaks. Rather, it only displays peaks below m/z 150, none of which were assignable to any characteristic fragment of Br_2Y. The various controls supported these results. The spectrum of PEM with CHCA displays only matrix-associated peaks. LD only of both Br_2Y-PEM and neat PEM without the VUV laser showed no signal either with or without added CHCA matrix, indicating that direct ionization did not occur at these desorption laser peak power densities, which were similar to those used to analyze the pure Br_2Y films.

The inability to detect any Br containing species with 7.87 eV laser photoionization when no matrix was added raises the question of how much Br_2Y was actually adsorbed into the Br_2Y-PEMs. X-ray photoelectron spectra were recorded on equivalent Br_2Y-PEM samples and indicated a 0.7% bromine content, compared to a calculated value of 13% for a pure Br_2Y film. Thus, the Br_2Y-PEMs had ~5% of the total Br_2Y of pure films, yet no Br-containing species could be observed in the absence of matrix. This ~5% Br_2Y concentration was apparently insufficient to allow the cluster formation needed for 7.87 eV SPI under these desorption conditions. By contrast, the matrix facilitated desorption of pure Br_2Y clusters or mixed Br_2Y/CHCA/water clusters, all of which were expected to display ionization energies below the 7.87 eV photon energy (see above). The applied matrix on the PEM likely extracted some of the Br_2Y into a surface layer where it co-crystallized with Br_2Y and permitted matrix assisted laser desorption, as is thought to occur in standard MALDI-MS.[21]

Next, the ionizing photon energy was raised in an attempt to detect adsorbed Br_2Y in the Br_2Y-PEM without the addition of matrix. Br_2Y was detected by 11.5 eV synchrotron LDPI-MS, as manifested in the m/z 185.1 (V) and m/z 264.0 (III) peaks from the Br_2Y-PEM (see Supporting Information). Experiments were performed in which the desorption laser peak power density was increased, but it neither enhanced the useful III/V fragment signal nor brought out any other peaks that were clearly characteristic of Br_2Y (data not shown). Rather, higher desorption laser peak power densities only led to more PEM degradation as characterized by pyrolysis peaks appearing at almost every integer m/z value up to ~m/z 450.

C. SIMS of Br_2Y Films, neat PEMs, and Br_2Y-PEMs. Films of Br_2Y, neat PEMs, and Br_2Y-PEMs were also analyzed by 25 keV Bi_3^+ SIMS. While the positive ion spectra were relatively uninteresting (see Supporting Information), the negative ion SIMS of the Br_2Y films and Br_2Y-PEMs in Figure 5 display significant useful signal.

The negative ion SIMS of the Br_2Y films displayed the $[Br_2Y]^-$ parent ion at m/z 336.9 and a strong Br^- peak at m/z 78.9. Several other Br_2Y-related peaks also appeared including one at m/z 262.9 that was similar to the structure III (see Figure 2) minus a proton. Other Br_2Y characteristic ions appeared at m/z 249.9 and m/z 275.9 and were attributed to the III structure either without the CH_2 group or with an additional CH_2 group, respectively. The clusters of peaks near m/z 290 were attributed to an overlap of the II ion and the II ion minus a proton. Finally, the peak at m/z 417.8 also appeared related to Br_2Y and was tentatively assigned to $[Br_2Y{\cdot}HBr]^-$, although at least one other assignment related to dimerized fragments of Br_2Y was also feasible.

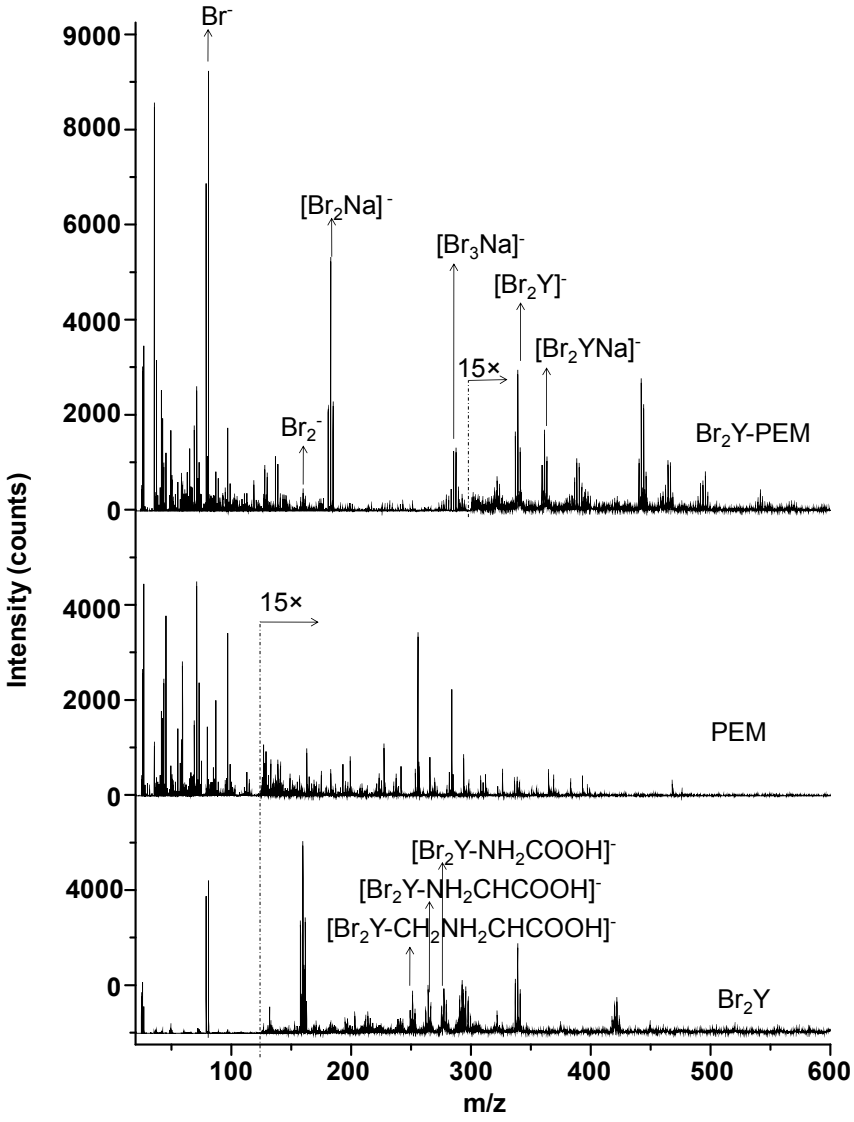

Figure 5. 25 keV Bi_3^+ SIMS negative ion spectra of a Br_2Y film, neat PEM, and Br_2Y-PEM.

The Br_2Y-PEMs also displayed the $[Br_2Y]^-$ parent ion and Br^-, but did not display the structurally intact (II, III, and related) fragments of Br_2Y that were observed for the negative ion SIMS of the neat Br_2Y films. However, other Br-containing ions were observed including m/z 157.8 corresponding to Br_2^-, m/z 180.8 corresponding to $[Br_2Na]^-$ and m/z 283.5 corresponding to $[Br_3Na]^-$. Br_2Y-PEM also showed a peak at m/z 359.4 assigned to $[Br_2Y][Na]^-$ and several other peaks up to m/z 550 with characteristic bromine isotopic patterns indicative of other $[Br_2Y][Na_xBr_y]^-$ or $[Na_xBr_y]^-$ structures. Thus, some of the most prominent ions in the negative

ion SIMS of the Br_2Y-PEMs showed high sensitivity to Br, but atomic $[Na_xBr_y]^-$ clusters contained little information on the analyte's chemical structure. That these various negative ion adducts containing Na appeared only in the Br_2Y-PEM spectra was attributed to the presence of excess sodium from the sodium alginate used in their preparation and/or a unique desorption event facilitated by the PEM (or the complexation of Br_2Y therein). The neat PEMs showed none of the above mentioned peaks associated with Br_2Y (see Figure 5).

IV. CONCLUSIONS

These results demonstrated several points of significance to the application of VUV SPI to MS imaging. It has usually been considered necessary for the VUV photon energy to exceed a molecular analytes' ionization energy to allow SPI.[10] However, the lower ionization energy of pure analyte, analyte/solvent, or analyte/matrix clusters that form during laser desorption can permit SPI at lower photon energies.[26,27,36] The practical implication of this observation is that the fluorine excimer laser might be much more widely useful for VUV postionization in MS imaging, as it can detect some species with ionization energies above its 7.87 eV photon energy when they cluster.

Cluster formation does require a relatively high density of gaseous species that was laser desorbed only from pure films or polyelectrolyte multilayers pretreated with matrix. Thus, even the relatively high (~5%) fraction of adsorbed Br_2Y in the polyelectrolyte multilayers was insufficient to produce clusters upon laser desorption unless CHCA matrix was added prior to analysis. The application of matrix was thought to facilitate extraction of adsorbed Br_2Y from within the multilayer while also enhancing the explosive desorption known to occur in MALDI.[20,21] Desorption was enhanced by matrix even though desorption laser peak power

density was kept low enough to minimize direct ion formation. Nevertheless, Br_2Y was detectable from multilayers when using higher photon energies.

The positive ion spectra from Bi_3^+ SIMS produced few useful results for these samples, showing mostly monomers of the polysaccharides (see Supporting Information).[37,38] However, the negative ion spectra were analytically quite useful. Like many organohalides, Br_2Y has a high electron affinity, which is expected to enhance negative ion formation.[39] However, most non-halogenated analytes have low electron affinities and may not produce as useful a negative signal. Furthermore, there was a strong dependence of the analyte's condensed phase environment upon the negative ion signal, with the neat films displaying major differences from the multilayer spectra. Overall, this particular analyte system displays complementary chemical information from LDPI-MS and SIMS, which is especially important as the latter is sometimes dominated by lower mass, fragmented ions. Finally, SIMS permits much higher spatial resolution for MS imaging of ~100 nm, compared with a spatial resolution of ~20 μm for LDPI-MS, similar to that observed for MALDI-MS.[40]

ACKNOWLEDGMENTS

The authors acknowledge the assistance of Jerry F. Moore and Oleg Kostko with various aspects of the data collection and analysis. This work is supported by the National Institute of Biomedical Imaging and Bioengineering via grant EB006532. The contents of this manuscript are solely the responsibility of the authors and do not necessarily represent the official views of the National Institute of Biomedical Imaging and Bioengineering or the National Institutes of Health. MA, LT, JZ and the Advanced Light Source are supported by the Director, Office of Energy Research, Office of Basic Energy Sciences, Chemical Sciences Division of the U.S. Department of Energy under contract No. DE-AC02-05CH11231.

SUPPORTING INFORMATION

The following figures and associate text are provided in the Supporting Information.

Figure S1. Preparation of the PEMs up to first dual layer of chitosan and alginate.

Figure S2. Preparation of PEMs consisting of a total of ten layers each of chitosan and alginate, some with Br_2Y adsorbed into every alternating alginate layer.

Figure S3. Attenuated total reflection Fourier transform infrared (ATR-FTIR) spectra of the alginate and chitosan peaks from a single layer of each.

Figure S4. ATR-FTIR spectra of PEMs of two, five, and fifteen layers.

Figure S5. Photoionization efficiency curve for Br_2Y thermally desorbed from pure film.

Figure S6. 9.45 and 11.5 eV photon energy SPI-MS of Br_2Y using synchrotron radiation.

Figure S7. Optimized geometry of Br_2Y from electronic structure calculations.

Figure S8. Optimized geometry of $[Br_2Y]_2$.

Figure S9. Optimized geometry of $[Br_2Y][H_2O]$.

Figure S10. Optimized geometry of $[Br_2Y][H_2O]_3$.

Figure S11. LDPI-MS of Br_2Y films recorded with 8.0 - 12.5 eV synchrotron photon energies.

Figure S12. 11.5 eV synchrotron LDPI-MS of Br_2Y-PEMs and neat PEMs.

Figure S13. Positive ion 25 keV Bi_3^{2+} SIMS of PEM and Br_2Y-PEM.

REFERENCES

(1) Otto, M. *Nat. Rev. Microbiol.* **2009**, *7*, 555.

(2) Tyler, B. J.; Rangaranjan, S.; Möller, J.; Beumer, A.; Arlinghaus, H. F. *Appl. Surf. Sci.* **2006**, *252*, 6712.

(3) Wucher, A.; Cheng, J.; Winograd, N. *Anal. Chem*. **2007**, *79*, 5529.

(4) Fletcher, J. S. *Analyst* **2009**, *134*, 2204.

(5) Esquenazi, E.; Yang, Y.-L.; Watrous, J.; Gerwick, W. H.; Dorrestein, P. C. *Nat. Prod. Rep.* **2009**, *26*, 1521.

(6) Akhmetov, A.; Moore, J. F.; Gasper, G. L.; Koin, P. J.; Hanley, L. *J. Mass Spectrom*. **2010**, *45*, 137.

(7) Gasper, G. L.; Takahashi, L. K.; Zhou, J.; Ahmed, M.; Moore, J. F.; Hanley, L. *Anal. Chem*. **2010**, *82*, 7472.

(8) Takahashi, L. K.; Zhou, J.; Wilson, K. R.; Leone, S. R.; Ahmed, M. *J. Phys. Chem. A* **2009**, *113*, 4035.

(9) Zhou, J.; Takahashi, L. K.; Wilson, K. R.; Leone, S. R.; Ahmed, M. *Anal. Chem*. **2010**, *82*, 3905.

(10) Hanley, L.; Zimmermann, R. *Anal. Chem*. **2009**, *81*, 4174.

(11) Li, Y.; Qi, F. *Acc. Chem. Res.* **2009**, *43*, 68.

(12) Gasper, G. L.; Takahashi, L. K.; Zhou, J.; Ahmed, M.; Moore, J. F.; Hanley, L. *Nucl. Instr. Meth. Phys. Res. A* **2011**, *in press*.

(13) Sostarecz, A. G.; Sun, S.; Szakal, C.; Wucher, A.; Winograd, N. *Appl. Surf. Sci.* **2004**, *231/232*, 179.

(14) Kozole, J.; Szakal, C.; Kurczy, M.; Winograd, N. *Appl. Surf. Sci.* **2006**, *252*, 6789.

(15) Deng, T.; Wang, H.; Li, J.; Hu, S.; Shen, G.; Yu, R. *Sens. Actuat. B* **2004**, *99*, 123.

(16) Heimann, P. A.; Koike, M.; Hsu, C. W.; Blank, D.; Yang, X. M.; Suits, A. G.; Lee, Y. T.; Evans, M.; Ng, C. Y.; Flaim, C.; Padmore, H. A. *Rev. Sci. Instrum*. **1997**, *68*, 1945.

(17) Maurstad, G.; Morch, Y. A.; Bausch, A. R.; Stokke, B. T. *Carbohyd. Polym*. **2008**, *71*, 672.

(18) Crot, C. A.; Wu, C.; Schlossman, M. L.; Trainor, T. P.; Eng, P. J.; Hanley, L. *Lang.* **2005**, *21*, 7899.

(19) Frisch, M. J.; Trucks, G. W.; Schlegel, H. B.; Scuseria, G. E.; Robb, M. A.; Cheeseman, J. R.; Montgomery, J. A. J.; Vreven, T.; Kudin, K. N.; Burant, J. C.; Millam, J. M.; Iyengar, S. S.; Tomasi, J.; Barone, V.; Mennucci, B.; Cossi, M.; Scalmani, G.; Rega, N.; Petersson, G. A.; Nakatsuji, H.; Hada, M.; Ehara, M.; Toyota, K.; Fukuda, R.; Hasegawa, J.; Ishida, M.; Nakajima, T.; Honda, Y.; Kitao, O.; Nakai, H.; Klene, M.; Li, X.; Knox, J. E.; Hratchian, H. P.; Cross, J. B.; Adamo, C.; Jaramillo, J.; Gomperts, R.; Stratmann, R. E.; Yazyev, O.; Austin, A. J.; Cammi, R.; Pomelli, C.; Ochterski, J. W.; Ayala, P. Y.; Morokuma, K.; Voth, G. A.; Salvador, P.; Dannenberg, J. J.; Zakrzewski, V. G.; Dapprich, S.; Daniels, A. D.; Strain, M. C.; Farkas, O.; Malick, D. K.; Rabuck, A. D.; Raghavachari, K.; Foresman, J. B.; Ortiz, J. V.; Cui, Q.; Baboul, A. G.; Clifford, S.; Cioslowski, J.; Stefanov, B. B.; Liu, G.; Liashenko, A.; Piskorz, P.; Komaromi, I.; Martin, R. L.; Fox, D. J.; T.; Keith; Al-Laham, M. A.; Peng, C. Y.; Nanayakkara, A.; Challacombe, M.; Gill, P. M. W.; Johnson, B.; Chen, W.; Wong, M. W.; Gonzalez, C.; Pople, J. A. "Gaussian 03, Revision A.1," Gaussian, Inc., 2003.

(20) Rohlfing, A.; Leisner, A.; Hillenkamp, F.; Dreisewerd, K. *J. Phys. Chem. C* **2009**, *114*, 5367.

(21) Knochenmuss, R.; Zhigilei, L. V. *J. Mass Spectrom*. **2010**, *45*, 333.

(22) Jochims, H.-W.; Schwell, M.; Chotin, J.-L.; Clemino, M.; Dulieu, F.; Baumgärtel, H.; Leach, S. *Chem. Phys.* **2004**, *298*, 279.

(23) Schwell, M.; Jochims, H.-W.; Baumgärtel, H.; Dulieu, F.; Leach, S. *Planet. Space Sci.* **2006**, *54*, 1073.

(24) Edirisinghe, P. D.; Moore, J. F.; Calaway, W. F.; Veryovkin, I. V.; Pellin, M. J.; Hanley, L. *Anal. Chem*. **2006**, *78*, 5876.

(25) Zhang, L.; Pan, Y.; Guo, H.; Zhang, T.; Sheng, L.; Qi, F.; Lo, P.-K.; Lau, K.-C. *J. Phys. Chem. A* **2009**, *113*, 5838.

(26) Kinsel, G. R.; Knochenmuss, R.; Setz, P.; Land, C. M.; Goh, S.-K.; Archibong, E. F.; Hardesty, J. H.; Marynick, D. S. *J. Mass Spectrom*. **2002**, *37*, 1131.

(27) Kostko, O.; Bravaya, K.; Krylov, A.; Ahmed, M. *Phys. Chem*. *Chem*. *Phys.* **2010**, *12*, 2860.

(28) Belau, L.; Wilson, K. R.; Leone, S. R.; Ahmed, M. *J. Phys. Chem*. *A* **2007**, *111*, 10075.

(29) Barth, S.; Oncak, M.; Ulrich, V.; Mucke, M.; Lischke, T.; Slavicek, P.; Hergenhahn, U. *J. Phys. Chem*. *A* **2009**, *113*, 13519.

(30) Heinbuch, S.; Dong, F.; Rocca, J. J.; Bernstein, E. R. *J. Chem*. *Phys.* **2007**, *126*, 244301.

(31) Gamez, G.; Zhu, L.; Schmitz, T. A.; Zenobi, R. *Anal. Chem*. **2008**, *80*, 6791.

(32) Suits, A. G.; Heimann, P.; Yang, X.; Evans, M.; Hsu, C.-W.; Lu, K.-t.; Lee, Y. T.; Kung, A. H. *Rev*. *Sci. Instrum*. **1995**, *66*, 4841.

(33) Scaiano, J. C.; Barra, M.; Sinta, R. *Chem*. *Mater.* **1996**, *8*, 161.

(34) Huang, J.; Xu, D.; Francisco, J. S.; Jackson, W. M. *J. Chem*. *Phys.* **2003**, *118*, 3083.

(35) Hanley, L.; Kornienko, O.; Ada, E. T.; Fuoco, E.; Trevor, J. L. *J. Mass Spectrom*. **1999**, *34*, 705.

(36) Marchi, I.; Rudaz, S.; Veuthey, J. *Talanta* **2009**, *78*, 1–18.

(37) Tam, S. K.; Dusseault, J.; Polizu, S.; Menard, M.; Halle, J.-P.; Yahia, L. H. *Biomater.* **2005**, *26*, 6950.

(38) Sjovall, P.; Lausmaa, J.; Johansson, B.-L.; Andersson, M. *Anal. Chem*. **2004**, *76*, 1857.

(39) Harrison, A. G. *Chemical Ionization Mass Spectrometry*; CRC Press: Boca Raton, 1992.

(40) Chughtai, K.; Heeren, R. M. A. *Chem*. *Rev*. **2010**, *110*, 3237.

TABLE OF CONTENTS GRAPHIC

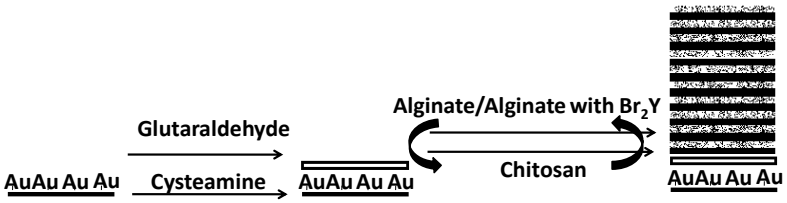

SUPPORTING INFORMATION FOR

Brominated Tyrosine and Polyelectrolyte Multilayer Analysis by Laser Desorption VUV Postionization and Secondary Ion Mass Spectrometry

Melvin Blaze M.T.[1], Lynelle K. Takahashi[2,3], Jia Zhou[3], Musahid Ahmed[3], F. Douglas Pleticha[1], and Luke Hanley[1,*]

[1]Department of Chemistry, University of Illinois at Chicago, Chicago, IL 60607
[2]Department of Chemistry, University of California, Berkeley, Berkeley, CA 94720
[3]Chemical Sciences Division, Lawrence Berkeley National Laboratory, Berkeley, CA 94720

S1. Preparation of PEMs. Polyelectrolyte multilayers (PEMs) with 10 alternating layers each of chitosan and alginate were prepared on gold-coated silicon substrates using cysteamine and glutaraldehyde as linkers by dip coating as shown in Figures S1 and S2.

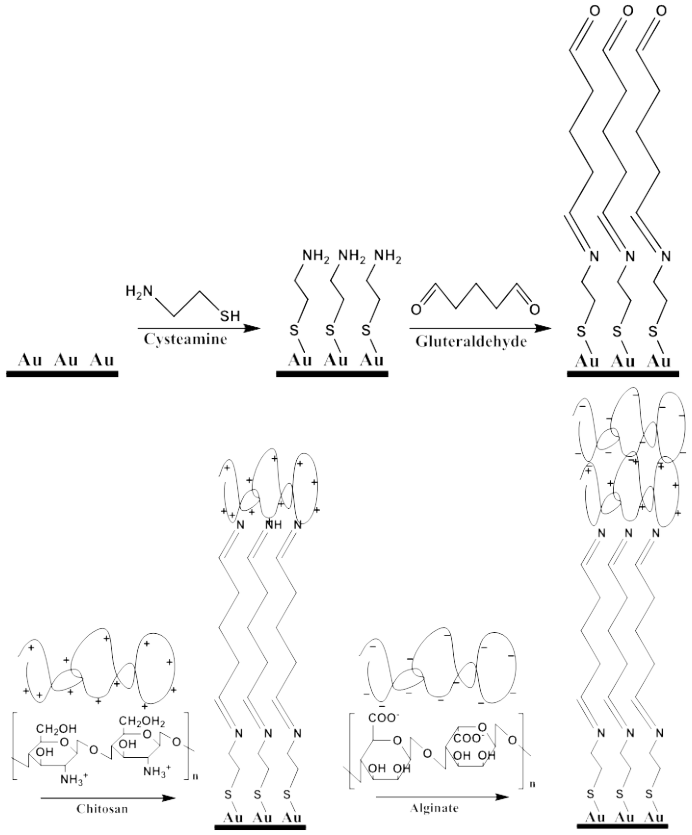

Figure S1. Preparation of polyelectrolyte multilayers (PEMs), up to first dual layer of chitosan and alginate.

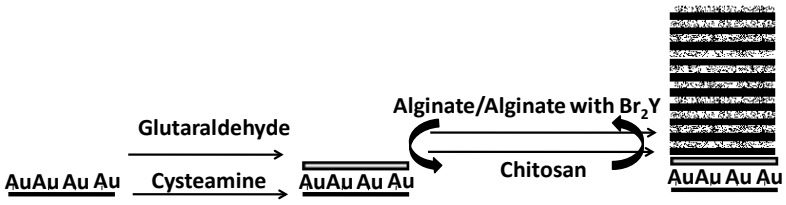

Figure S2. Preparation of PEMs consisting of a total of ten layers each of chitosan and alginate, some with 2,5-dibromotyrosine (Br_2Y) adsorbed into every alternating alginate layer (Br_2Y-PEMs).

PEM2 were prepared by a method described previously.[15,17] The Au substrate was first cleaned by sonication in piranha solution consisting of (7:3 v:v) concentrated sulfuric acid:30% hydrogen peroxide, then rinsed several times with distilled water. A cysteamine solution was used to prepare a self-assembled monolayer on the gold surface, which was then reacted with a glutaraldehyde solution that covalently bound the first polysaccharide layer of chitosan. The modified substrate was then manually immersed alternately in chitosan solution (0.2% w:v dissolved in 2% v:v acetic acid solution) and sodium alginate (2% w:v in water) for one hour each, with intermediate rinsing using deionized water. The resultant PEMs consisted of a total of ten alternating layers each of chitosan and alginate. Br_2Y was incorporated in every alternating layer of PEM as a zwitterion mixed with the unmodified alginate solution to form the Br_2Y-PEM (see Figure S2).

S2. Verification of PEMs. PEMs were verified by attenuated total reflection Fourier transform infrared spectroscopy (ATR-FTIR). ATR-FTIR spectra were acquired (ABB FTLA2000 spectrometer) with a germanium ATR crystal by collecting 120 scans at 2 cm^{-1} resolution with a wavenumber range of 4600 - 500 cm^{-1}. Background spectra were recorded using a gold-coated substrate cleaned with piranha solution. Spectral manipulations were performed using commercial analysis software (GRAMS/32). Figure S3 shows the ATR-FTIR spectra for a PEM with single alternating layers of chitosan and alginate which displays peaks characteristic to chitosan and alginate. Figure S4 shows the ATR-FTIR spectra for PEMs with

two, five, and fifteen layers: more layers show higher intensity of peaks characteristic to chitosan and alginate, confirming the formation of PEMs.

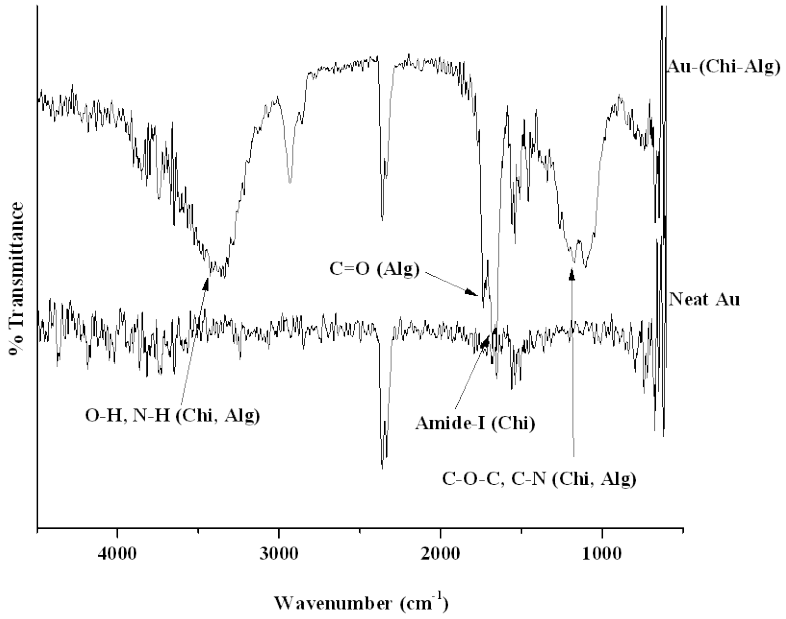

Figure S3. ATR-FTIR spectra showing alginate and chitosan characteristic peaks from (top) single alternating layers of alginate and chitosan on Au. Also shown (bottom) is the ATR-FTIR of a clean Au substrate.

The fully prepared PEMs were also analyzed by monochromatic X-ray photoelectron spectroscopy using instrumentation and procedures previously described.[18] Elemental content was determined by peak fitting the carbon *1s*, nitrogen *1s*, oxygen *1s* and bromine $3d_{5/2}$ core level X-ray photoelectron spectra using commercial software (XPS Peak 4.1) after correcting for elemental dependences on photoionization cross section.

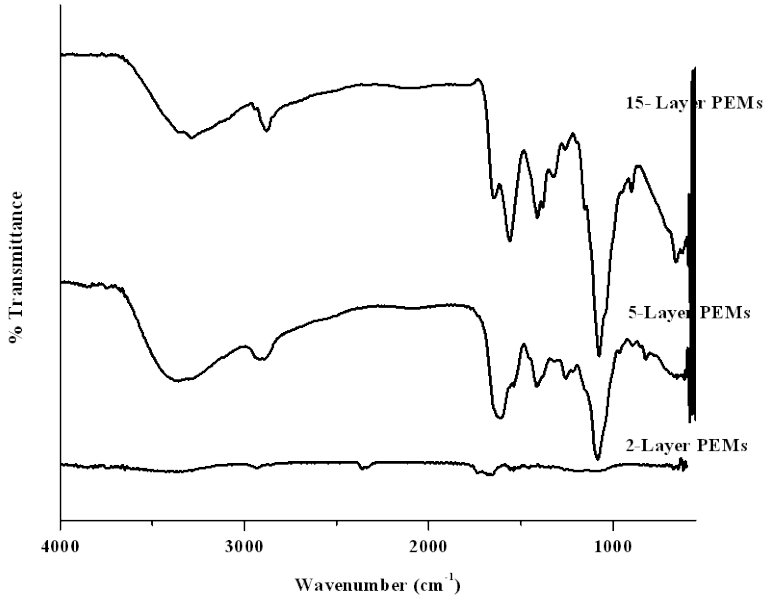

Figure S4. ATR-FTIR spectra of PEMs of two, five, and fifteen layers.

S3. 8 – 12.5 eV Synchrotron LDPI-MS and SIMS. Synchrotron LDPI-MS and SIMS were recorded using a commercial SIMS instrument (TOF.SIMS 5, ION-TOF Inc., Munster, Germany) equipped with a bismuth liquid metal ion gun emitting 25 keV Bi_3^+ pulses at 10 kHz.[8] The SIMS instrument was modified for LDPI-MS by the addition of a 349 nm pulsed desorption laser (Explorer, Newport) operating at 2500 Hz with a spot size of ~30 μm diameter and typical laser desorption peak power density of 1 to 10 MW/cm^2. The laser desorbed neutral molecules were photoionized by 8.0 to 12.5 eV tunable VUV synchrotron radiation from the Chemical Dynamics Beamline at the Advanced Light Source (Lawrence Berkeley National Laboratory, Berkeley, CA)[16] The photoionized neutrals were extracted using a 5 μs extraction pulse with a delay time of 1.2 – 1.4 μs with respect to the desorption pulse. 143,000 laser shots on a single spot were used for each displayed mass spectrum.

This instrument was also used to record photoionization efficiency curves of gas phase Br_2Y molecules by thermally heating the sample above 120°C while scanning the VUV photon energy, without any ion or laser desorption.

S4. 7.87 eV Laser LDPI-MS. 7.87 eV laser LDPI-MS was collected using a custom built instrument at the University of Illinois at Chicago which is equipped with a 157.6 nm pulsed laser for photoionization and was described in detail previously.[6] This LDPI-MS has a 349 nm Nd:YLF desorption laser operating at 100 Hz, with a spot size of ~20 μm diameter and typical desorption laser peak power density ranging from 30 to 70 MW/cm^2. The sample was rastered at 100 μm/s with respect to the laser, so each 20 μm sample spot was sampled by ~20 desorption laser shots and a total of 50 – 100 laser shots were sufficient to obtain spectra with optimal signal to noise. The desorbed neutral molecules were photoionized using a 157.6 nm (7.87 eV) molecular fluorine excimer laser operating at a 100 Hz with a spot size of approximately 8 mm in the ionization region and an energy of ~100 μJ/pulse. The photoionized neutrals were extracted using a pseudo-orthogonal delayed pulsed extraction and detected by a home-built two-stage reflectron time of flight mass spectrometer. Spectra were recorded at a delay of 3.9 μs between the photoionization laser and the extraction pulse. Varying this delay by a few μs affected the absolute signal, but not the overall appearance of the spectra. The instrument was also equipped with an ultrahigh vacuum compatible translation stage for sample manipulation and a digital single lens reflex camera for real time sample viewing on a high definition television. Data acquisition and sample stage movements were computer controlled using customized software.

S5. Single Photon Ionization (SPI) MS of Evaporated Br_2Y. The data in Figure S5 displays the relative $[Br_2Y]^+$ parent ion signal from evaporated Br_2Y as a function of photon energy as a function of synchrotron photon energies. Full SPI-MS were recorded at each photon energy point on the curve in Figure S5 and two of these spectra, recorded at 9.45 and 11.5 eV photon energies, are shown in Figure S6. 9.45 eV corresponds to ~1.1 eV internal energy deposited into the parent ion (the photon energy minus the ionization energy) while 11.5 eV corresponds to ~3.2 eV internal energy in the parent ion. The increase in internal energy significantly enhanced fragmentation in the parent ion at the higher photon energy, as expected.

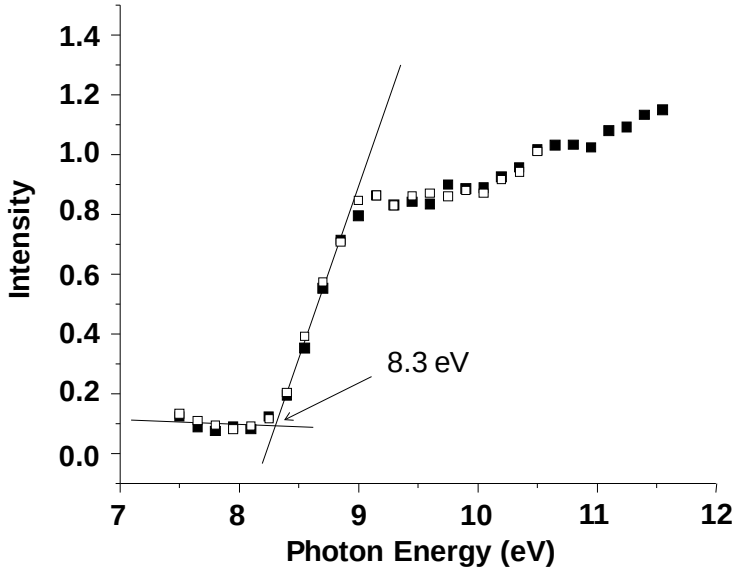

Figure S5. Photoionization efficiency curve for Br_2Y thermally desorbed from pure films recorded by sweeping the VUV photon energy while monitoring the m/z 337 parent ion. Intensities normalized to data collected at 10.5 eV photon energy. Lines are extrapolations indicating 8.3±0.1 eV experimental ionization energy. The different symbols correspond to different runs.

Several of the fragments observed in SPI-MS of evaporated Br_2Y are similar to those from LDPI-MS of Br_2Y films (see Figure 1). Specifically, the II, III, and V fragments identified in Figure 2 were observed along with the parent ion by SPI-MS and ≤8.0 eV LDPI-MS. However, little to none of the I, V, and VI fragments observed by LDPI-MS were detected by

SPI-MS. Furthermore, SPI-MS additionally detected a deprotonated III fragment ion, denoted as $[III-H]^+$ in Figure S6, which was not observed at all in LDPI-MS. There were also significant differences in the fragment/parent ion ratios between LDPI-MS and SPI-MS: the (II/parent) and (III/parent) ratios were much higher in LDPI-MS than in SPI-MS, indicating a greater extent of fragmentation in the former and differences in fragmentation mechanisms between the two cases. Finally, there were no cluster ions observed by SPI-MS, unlike the case for LDPI-MS (Figure 3).

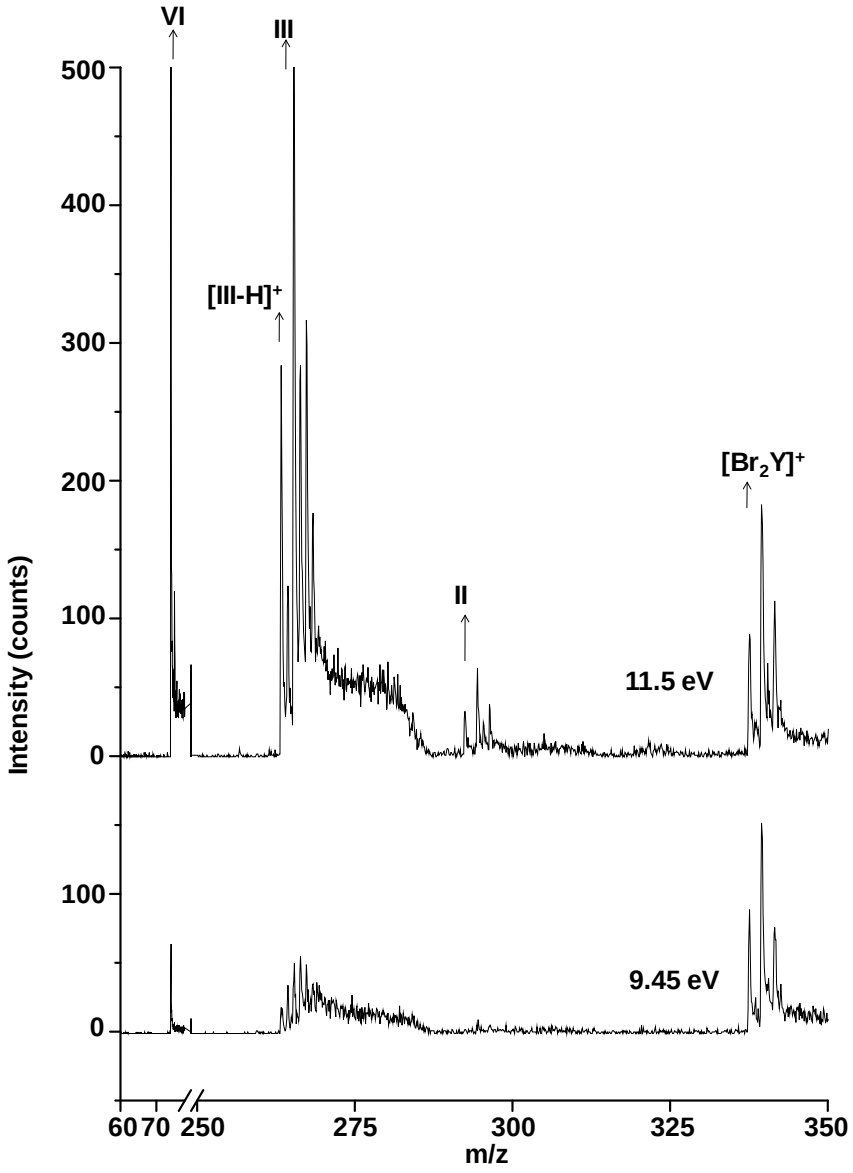

Figure S6. 9.45 and 11.5 eV photon energy SPI-MS of Br_2Y using synchrotron radiation.

S6. Geometries Used for Electronic Structure Calculation of Ionization Energies. Ionization energies (IEs) of Br_2Y , $[Br_2Y]_2$, [Br2Y][H2O] and $[Br2Y][H2O]_3$ were calculated using density functional theory in Gaussian 03.[19] The optimized geometries in the ground state shown in Figures S7 – S10 were used to calculate the vertical IEs by freezing the geometries and removing one electron from the highest occupied molecular orbital All calculations were performed at the B3LYP/6-311+G** level and were corrected for zero point energy on the structures shown in the Supporting Information that represented local minima on their respective potential energy surfaces.

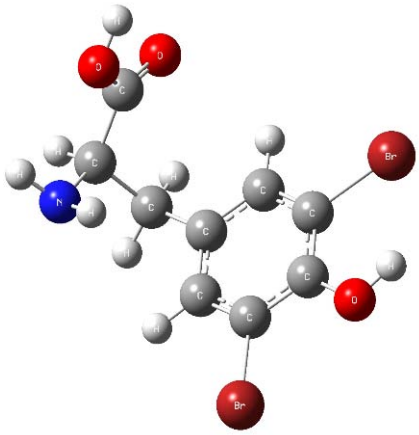

Figure S7. Optimized geometry of Br_2Y.

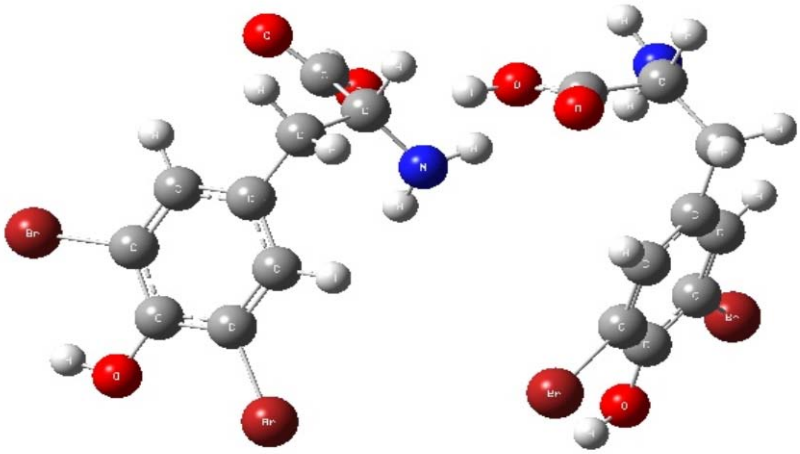

Figure S8. Optimized geometry of $[Br_2Y]_2$.

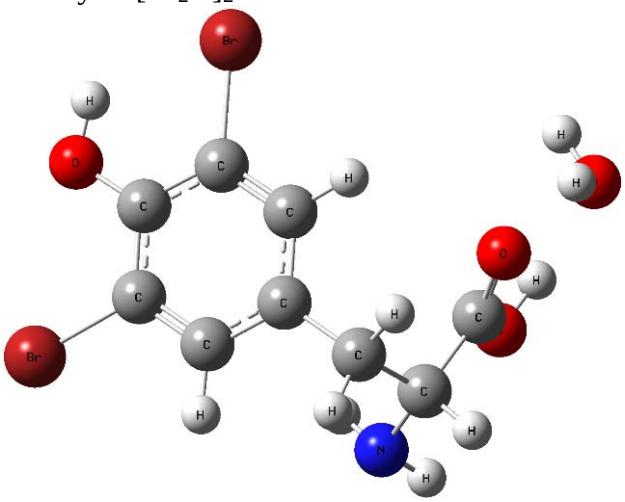

Figure S9. Optimized geometry of $[Br_2Y][H_2O]$.

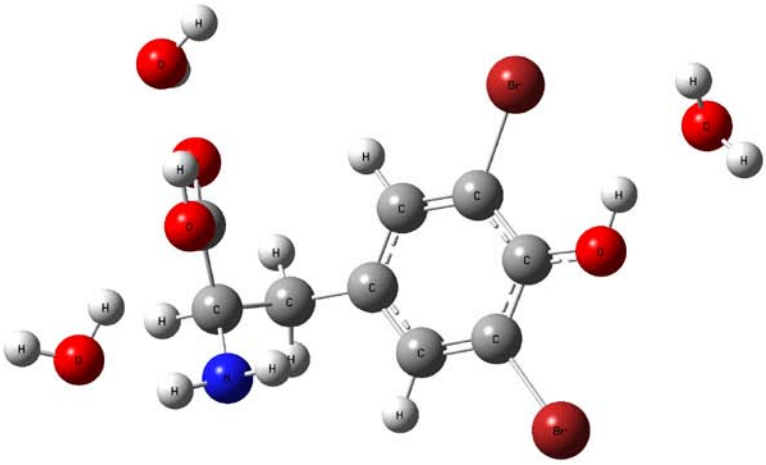

Figure S10. Optimized geometry of $[Br_2Y][H_2O]_3$.

S7. LDPI-MS of Br_2Y films, PEMs, and Br_2Y-PEMs at Higher Photon Energies.

See main text for discussion of these figures.

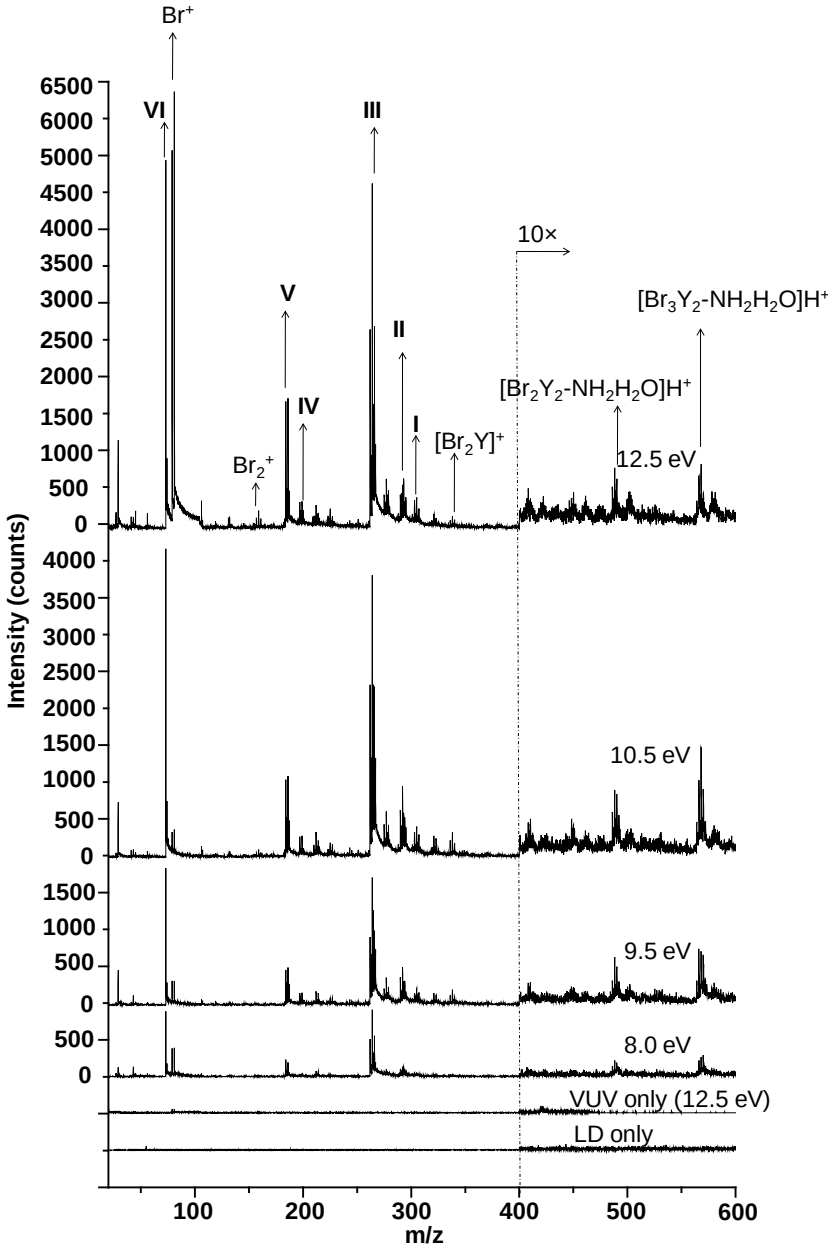

Figure S11. LDPI-MS of Br_2Y films recorded with 8.0 - 12.5 eV photon energies produced at the synchrotron. The "VUV only" spectrum was recorded with 12.5 eV photons, but without laser desorption while the "LD only" spectrum is recorded with the desorption laser but without any photoionization.

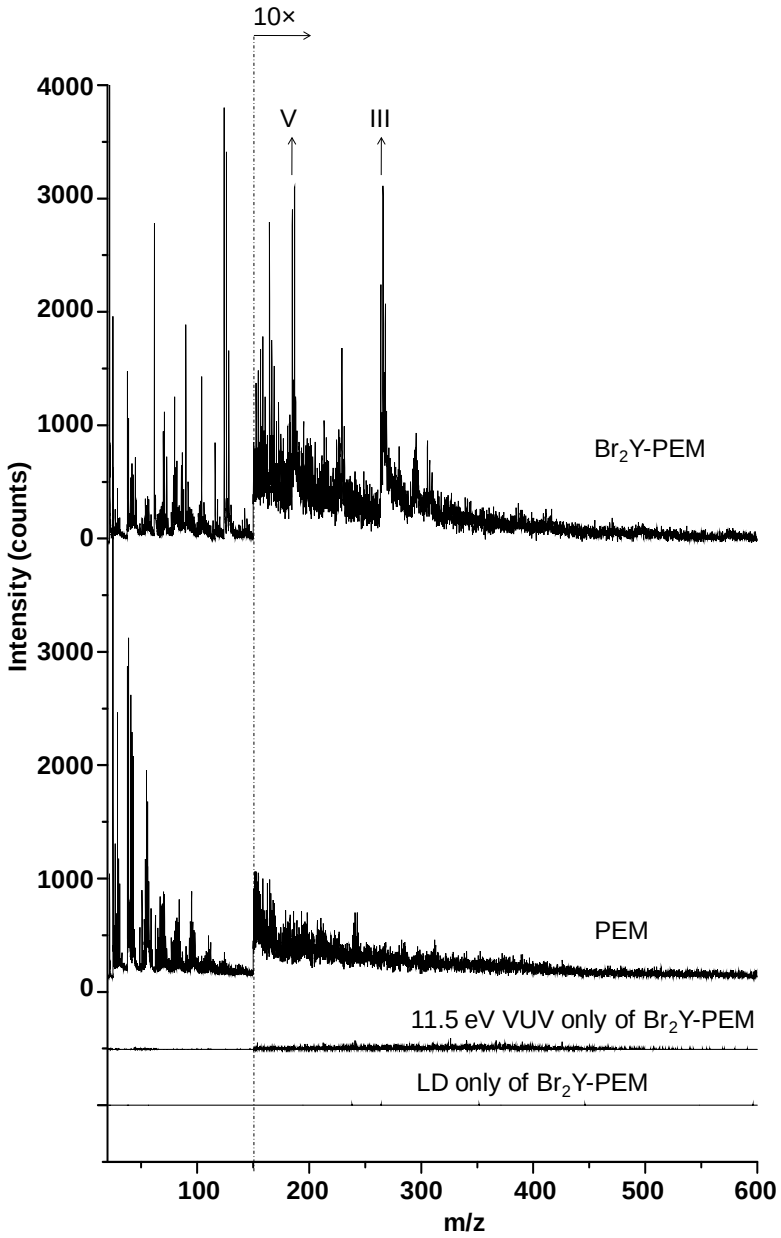

Figure S12. 11.5 eV synchrotron LDPI-MS of Br_2Y-PEMs and neat PEMs. The 11.5 eV SPI-MS and LD only mass spectra for Br_2Y-PEMs are also shown.

S8. Positive Ion SIMS of PEMs and Br_2Y-PEMs. Neat PEMs and Br_2Y-PEMs were also analyzed by 25 keV Bi_3^+ SIMS and the positive ion spectra are shown in Figure S13. Both spectra show several peaks that are characteristic to chitosan and alginate fragments: the peak at m/z 199.1 was attributed to the $[C_6H_8O_6Na]^+$ alginate monomer, m/z 125 to the $[C_3H_2O_4Na]^+$ alginate fragment, and m/z 97.2 to $[C_6H_9O]^+$ from both chitosan and alginate.[37,38] Higher mass

(as yet unidentified) fragments were also observed at m/z 250.2 and m/z 275, with additional lower mass peak groups below m/z 100 resulting from extensive chitosan/alginate degradation. However, SIMS of the Br_2Y-PEMs showed no evidence for the presence of Br^+ in the multilayer, where the vertical lines in the inset indicate where $^{79}Br^+$ and $^{81}Br^+$ would appear. Even the Br^+ region did not display any signal unique to the Br_2Y-PEM. While the Br_2Y-PEM did show unique peaks at m/z 111.6 and 137.8, these lacked the characteristic isotopic distribution for bromine and therefore could not have resulted solely from any Br-containing fragments of Br_2Y.

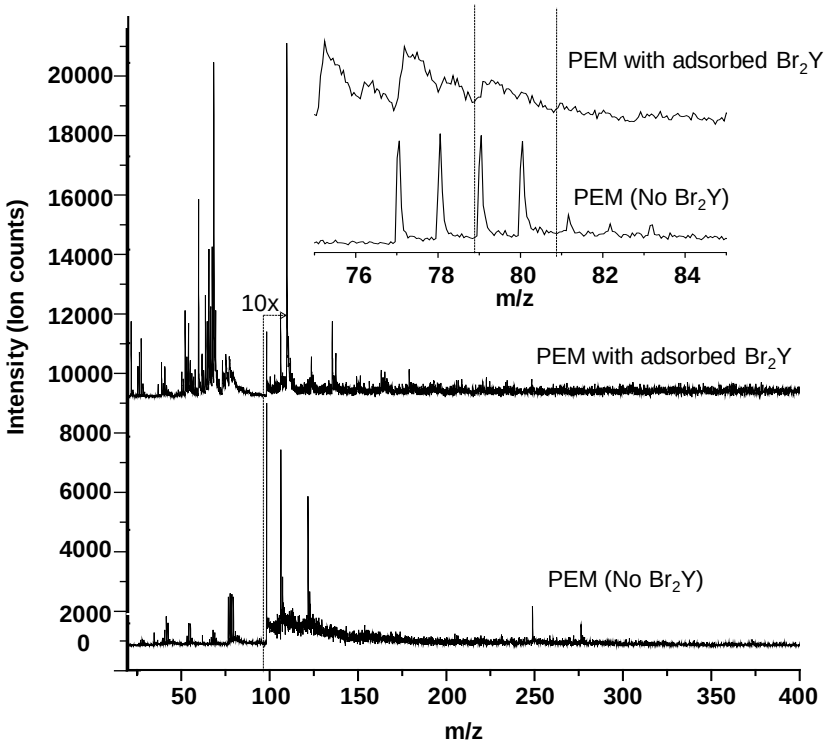

Figure S13. Positive ion 25 keV Bi_3^{2+} SIMS of PEM and Br_2Y-PEM. Vertical lines in inset indicate where $^{79}Br^+$ and $^{81}Br^+$ would appear.

DISCLAIMER